npj | Flexible Electronics

www.nature.com/npjflexelectron

ARTICLE OPEN

Check for updates

Superelastic alloy based electrical interconnects for highly stretchable electronics

Yangyong Zhao[1,4], Weifan Zhou[1,4], Yixiang Shi[1], Xianqing Yang[1], Yuanyuan Bai[1], Lianhui Li[1], Shuqi Wang[1], Tie Li[1,2], Simin Feng[1] and Ting Zhang[1,2,3]✉

To achieve stretchable inorganic electronics, improving elastic stretchability of the electrical interconnects becomes a bottleneck needed to be addressed. Here, we propose a material of Ni-Ti superelastic alloy for the design and fabrication of deformable interconnects, whose intrinsic elastic property overcomes the low intrinsic elastic strain limit of conventional metals. The serpentine interconnect made by Ni-Ti alloy with an intrinsic elastic strain limit of ~7.5% represents a much higher elastic stretchability than conventional Cu interconnect. The deformation behavior of the interconnect is systematically investigated through finite element analysis (FEA) simulations and experiments. The results reveal that the interconnect exhibits an elastic stretchability up to 196%, and its resistance only changes by 0.4% with 100% strain. Moreover, the potentials and challenges of other superelastic alloys as electrical interconnects are discussed. The proposed superelastic alloys fundamentally boost the stretchable properties of electrical interconnects, which would open up opportunities for flexible and stretchable electronics.

npj Flexible Electronics (2022)6:8 ; https://doi.org/10.1038/s41528-022-00142-2

INTRODUCTION

Over the past decade, stretchable inorganic electronics based on structural design has developed rapidly[1–7]. A key to this strategy is to make non-stretchable inorganic materials into specific structures that can absorb the applied strain without fracturing[2]. The island-bridge structure design, where the discrete islands (rigid functional device components) adhered to the flexible substrates are connected by stretchable bridges (electrical interconnects), is a popular approach for stretchable electronics. Recently, several advanced stretchable circuits with this structural design have been demonstrated and applied to stretchable batteries[7], biomedical wearable devices[3,8], and stretchable sensors[9]. According to the way of encapsulation, the electrical interconnects can be classified into two categories, including free-standing designs housed in microfluidic enclosures[3,7] and those embedded in the flexible substrate[6,8]. No matter what kind of encapsulation, the elastic stretchability, defined by the condition in which the interconnect can return to its initial configuration after the applied strain is released, determines the safe stretchable strain of the entire device[10]. Once the applied strain exceeds the elastic stretchability, plastic deformation will occur in the material, which would result in interconnects entanglement for the free-standing designs[7,10] or rapid fatigue fracture of interconnects for those embedded designs[11,12]. Therefore, improving the elastic stretchability of the interconnects is very important in the flexible and stretchable electronics research field.

The elastic stretchability of the interconnect is mainly determined by two factors: (1) the geometric structure of the interconnect, (2) the elastic strain limit of the material[1,2,10]. Up to now, research reports on increasing the elastic stretchability of interconnects are usually considered from the perspective of structural design, which could reduce the strain level in the material for stretching[4,5,7]. In the past few years, the geometric structure has evolved from simple geometry of arc-shaped structure[13] to complex geometric shapes, such as serpentine[6,10], self-similar[4,5,7], 2D spiral[14], and 3D helical forms[15,16]. However, whatever the structure, the low intrinsic elastic strain limit of conventional metals (e.g., only 0.3% for copper) fundamentally impedes its stretchable performance. The elastic strain limit, as large as the yield strain, ε_{yeild}, is less than 0.5% for conventional metals as shown in the left of Fig. 1c. During stretching of the interconnects made by conventional metals, once the maximum principal strain in the material, ε_{max}, exceeds its elastic strain limit, ε_{ela}, irreversible plastic deformation will occur and lead to irreversible configuration[7,10]. Therefore, in order to improve the stretchable properties of electrical interconnects, it is crucial to explore a kind of materials with a higher elastic strain limit.

Different from conventional metals, superelastic alloys, i.e., shape memory alloys (SMAs) could exhibit a superelastic effect with a reversible strain larger than several percent (e.g., above 6% for Ni-Ti alloy) as illustrated in the right of Fig. 1c. Since the elastic strain limit of superelastic SMAs is much larger than that of conventional metals, it can be expected that the interconnect based on SMAs would have higher elastic stretchability. In the present study, typical superelastic Ni-Ti alloy is used to make the serpentine interconnect for stretchable electronics. The results indicate that compared with conventional metals, the elastic stretchability of interconnects could be significantly improved by Ni-Ti alloys with a rate of up to 196%. Detailed deformations, consisting of strain distribution and phase transformation of the Ni-Ti serpentine interconnects are systematically investigated through finite element analyses (FEA) simulations and experiments. Due to the low strain level and the localized characteristics of strain distribution in the interconnect, the electrical resistance only changes by 0.4% with 100% strain. The mechanical and electrical properties of Ni-Ti alloys facilitate its utilization as

[1]i-lab, Key Laboratory of Multifunctional Nanomaterials and Smart Systems, Suzhou Institute of Nano-Tech and Nano-Bionics (SINANO), Chinese Academy of Sciences (CAS), 398 Ruoshui Road, Suzhou 215123, P. R. China. [2]Gusu Laboratory for Materials Science, 388 Ruoshui Road, Suzhou 215123, P. R. China. [3]Center for Excellence in Brain Science and Intelligence Technology, Chinese Academy of Sciences, Shanghai 200031, P. R. China. [4]These authors contributed equally: Yangyong Zhao, Weifan Zhou. ✉email: tzhang2009@sinano.ac.cn

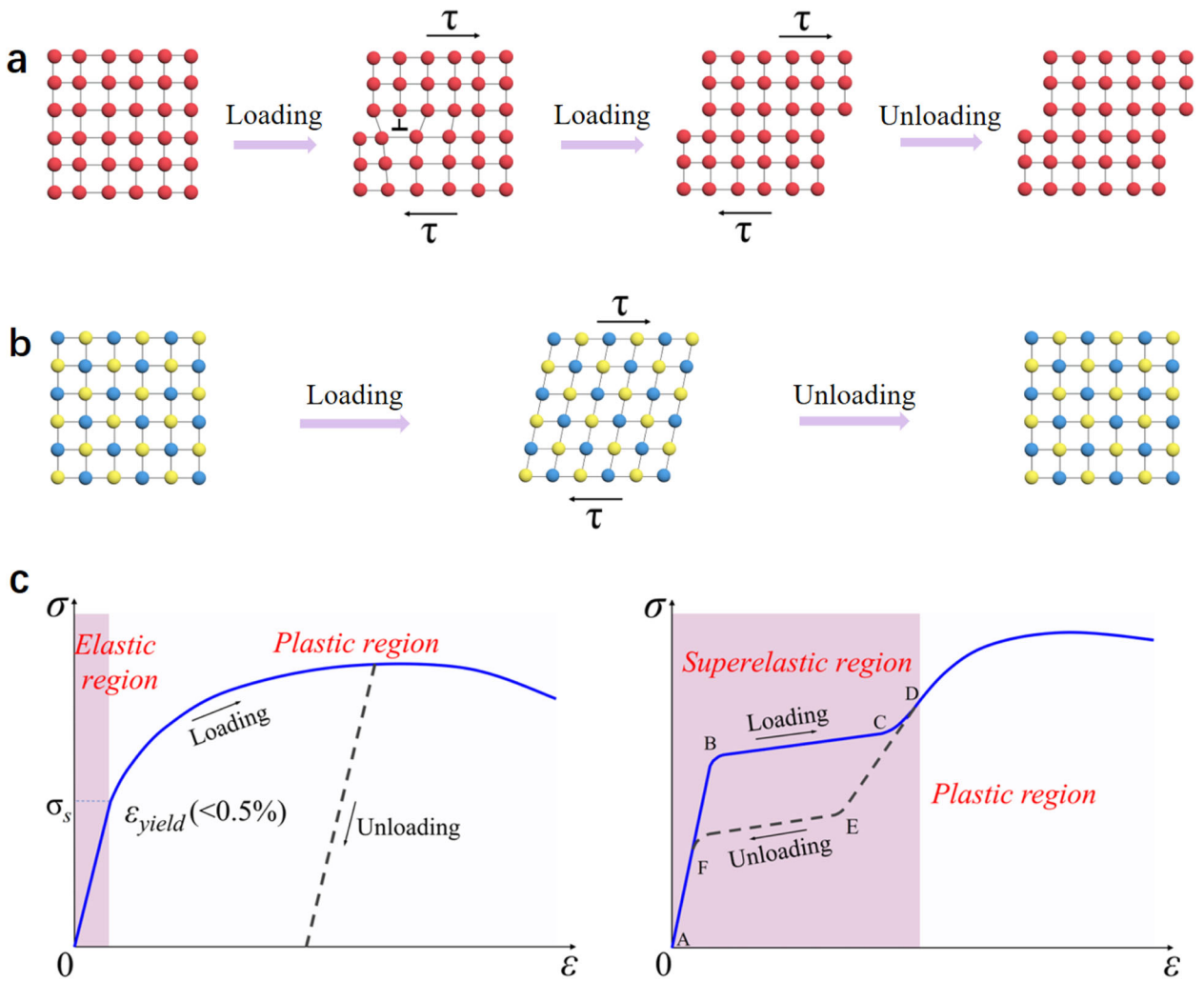

Fig. 1 Schematic diagram of deformation mechanism. Illustration of the micro-mechanism of deformation for irreversible dislocation slip for conventional metals (**a**) and reversible phase transformation for superelastic alloys (**b**), respectively. **c** Illustration of the elastic strain range for conventional metals (left) and superelastic shape memory alloys (right).

interconnects for stretchable electronics, as illustrated by light-emitting diodes (LEDs) assembled by Ni-Ti serpentine interconnects. This study introduces a material, which paves the way for highly stretchable interconnects design for future stretchable electronics.

RESULTS AND DISCUSSION

A comparison of elastic stretchability between Cu and Ni-Ti serpentine interconnects

The reversibility of serpentine interconnects based on Cu and Ni-Ti with the same diameter of 100 μm is compared. The dimensions of the serpentine interconnects are illustrated in Supplementary Fig. 1a, which consists of two arcs on each end and four half circles connected by five vertical straight lines. The formation process is shown in Fig. 2a, b (details in experiment section). During the mechanical test, one end of the interconnect is fixed and the other end is stretched to selected values of strain before it returns to its initial position. Supplementary Movie 1 (also see Fig. 2c) and Movie 2 show the deformation behavior of the interconnects with an applied strain of 100 and 182%, respectively. The Ni-Ti interconnect recovers fully, while the configuration of the Cu serpentine interconnect changes seriously after the applied strain is released. This means the applied strain is within the elastic range of the Ni-Ti serpentine interconnect, while irreversible plastic deformation occurs in the Cu serpentine interconnect. The plastic deformation in conventional metals originates from the irreversible dislocation slip mechanism, which is depicted in Fig. 1a. Dislocations are line defects of the crystal lattice which may move when subjected to critical stress, indicated as τ, thereby introducing a permanent shear of the lattice[17]. Different from conventional metals, the crystal structure of SMAs could reversibly transform between austenite and martensite upon loading and unloading as illustrated in Fig. 1b[18,19]. This deformation mechanism results in higher superelastic strain. The comparison results confirm the speculation that by increasing the intrinsic elastic strain limit of the material through the utilization of superelastic alloys, elastic stretchability of the interconnect could be improved significantly.

Mechanical properties of the Ni-Ti serpentine interconnects

In this section, we carried out experimental observations as well as FEA simulations to demonstrate the stretchability of the Ni-Ti serpentine interconnects. Before FEA simulations, mechanical and thermal properties of the Ni-Ti alloy are characterized. Firstly, in order to obtain the elastic strain limit of the Ni-Ti alloy, loading-unloading tests of a straight Ni-Ti wire with different applied tensile strains are performed at room temperature in a dynamic mechanical analyzer (DMA). As shown in Fig. 3a, the applied strain

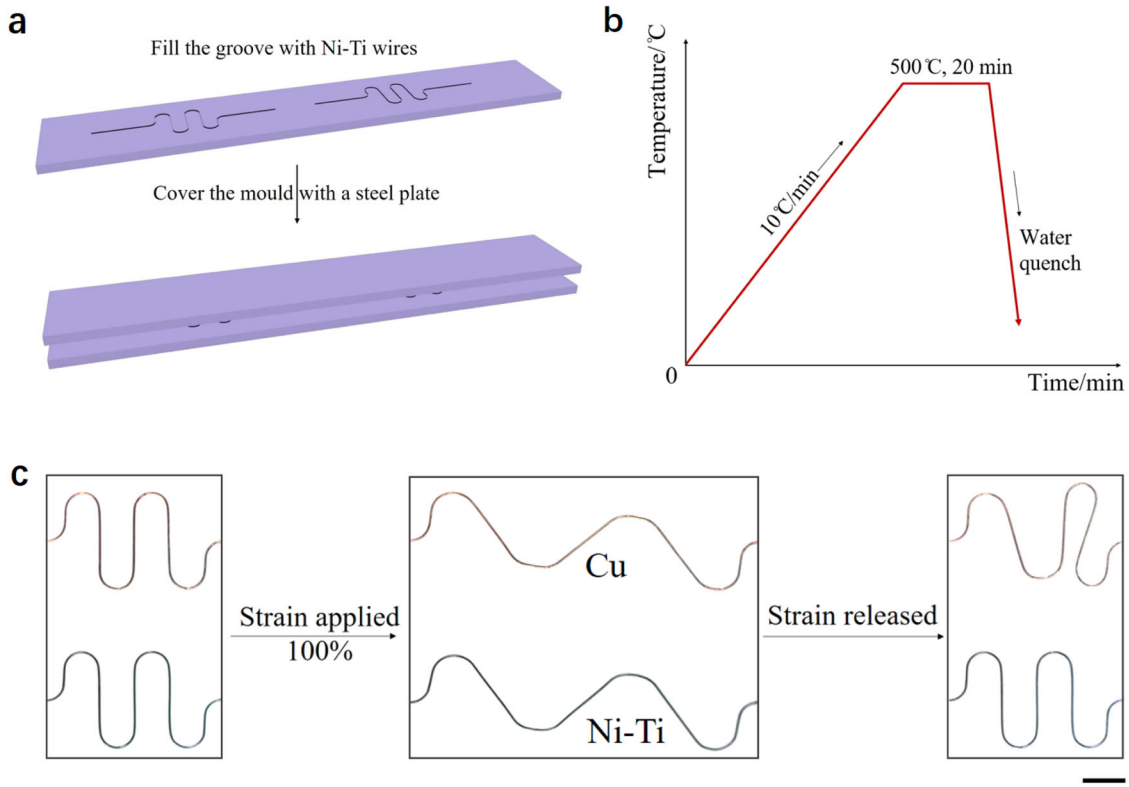

Fig. 2 Comparison of mechanical properties. a Schematic illustration of the formation process of the Ni-Ti serpentine interconnects by mold. **b** Diagram of the heat treatment for setting the Ni-Ti wires into serpentine interconnects. **c** A comparison of elastic stretchability between Cu and Ni-Ti serpentine interconnects. The right column shows the interconnect structures after releasing 100% applied strain. The scale bar is 2 mm.

is almost completely recovered after unloading when the applied strain is less than 7.5%, while about 1% residual strain is left when the applied strain is 10%. The residual strain after unloading is plotted as a function of applied strain as shown in Fig. 3b, from which it can be seen that the elastic strain limit of the Ni-Ti alloy is about 7.5%.

Furthermore, mechanical properties at different temperatures of Ni-Ti alloy are characterized by DMA as shown in Supplementary Fig. 3, from which the critical stresses to induce phase transformations are obtained and related mechanical parameters are calculated by linear fitting as shown in Fig. 3c (for more details see experiment section and Supplementary Fig. 4). Thermal differential scanning calorimetry (DSC) is carried out to characterize transformation temperatures as shown in Fig. 3d. All mechanical and thermal parameters for Ni-Ti alloy are instructed in Supplementary Table 1, and the experiment results are summarized in Supplementary Table 2.

Figure 4 shows the evolution of deformations for strains between 0 and 200% through experimental images and FEA results (see also Supplementary Movie 3). The dimension of the interconnect is illustrated in Supplementary Fig. 1b. The interconnect configurations predicted by FEA agree remarkably well with optical images for selected values of strain. Upon stretching of the structure, the arc and half-circle segments gradually extend and the straight parts mainly incline from vertical to horizontal direction with a little bending. Note also that during the whole deformation process, the stretching deformation of the Ni-Ti serpentine interconnects only occurs in the plane. The color in FEA results in Fig. 4 and Supplementary Movie 3 represents the distribution of the maximum principal strain in the material. It shows that initially the strain mainly concentrates in the arc and half-circle segments. When the interconnect was stretched to a strain of 120%, the localized strain in the arc and half-circle segments is very small and mainly concentrated in the surface of the interconnect. Until the serpentine structure approaches a straight line (with applied strain exceeding 185%), the strain in the material increases rapidly, which defines the elastic strain limit in stretchability.

Figure 5a plots ε_{max} in the material as a function of the applied strain, ε_{app}. For reversible behavior (that is, the interconnects return to its initial state after the release of strain), ε_{max} must be less than or equal to ε_{ela} of the material, which is 7.5% for the Ni-Ti alloy as demonstrated in Fig. 3b. Therefore, the elastic stretchability of the serpentine interconnect could be predicted to be 196%, which is in good agreement with the experimental observations, as the structure could fully recover after being released from 185% applied strain, while the structure configuration will have a slight change after released from the 200% applied strain (see Fig. 4 and Supplementary Movies 4, 5). This high elastic stretchability for the Ni-Ti interconnect could be explained by two factors, one of which rely on the design of serpentine structure which could reduce the strain level in the materials under stretching, while the other depends on the ultrahigh elastic strain limit of Ni-Ti alloy, which is much higher than conventional metals. The combined effect of these two factors makes the strain in the material lower than the elastic strain limit even under extreme stretching, thus greatly enhancing the elastic stretchability.

As mentioned previously, the large reversible strain in the superelastic SMAs comes from the reversible phase transformation between austenite and martensite. Supplementary Fig. 6 depicts the evolution of martensite volume fraction distribution with strains ranging from 0 to 200% through FEA simulations, which represents the degree of phase transformation from austenite to martensite. According to the spatial distribution and extent of phase transformation, the stretching deformation could be

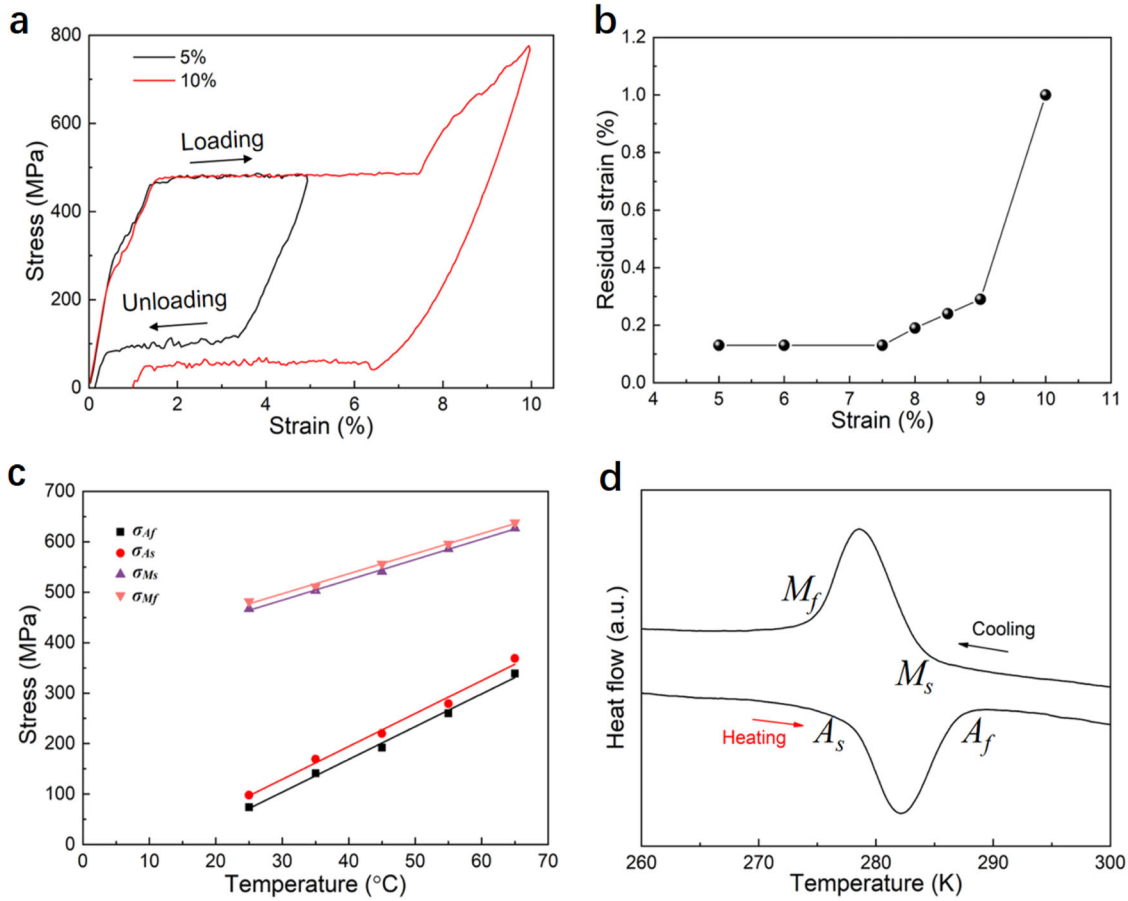

Fig. 3 Mechanical and thermal properties of Ni-Ti wires. a Loading-unloading stress-strain curves of the straight Ni-Ti wire with a diameter of 30 μm under various levels of applied tensile strain at room temperature. **b** The dependence of the residual strain on the applied tensile strain. **c** Linear fitting of the critical stresses versus temperature, the parameters C_M and C_A is defined by the slopes of the fitting line. **d** DSC measurement of the straight Ni-Ti wires at a heating/cooling rate of 5 °C/min, showing the transformation peaks.

divided into four stages. In the first stage, the entire structure only undergoes elastic deformation of austenite. When ε_{max} continues to increase and reaches the critical point, ε_M, the austenite to martensite transformation happens in the interconnect and the second stage comes. The value of ε_M could be obtained by the strain at the beginning of the platform in the tensile stress-strain curves of the Ni-Ti wire and estimated to be around 0.77% as shown in Fig. 3a. By putting this value back in Fig. 5a, we could extract the critical value of applied strain that initiates the martensite transformation as 54%. Similar to the evolution of ε_{max}, most of the transformation happens in the arc and half-circle segment areas. The second stage continues until the serpentine interconnect is stretched to 185% and approaching a straight line. The martensite volume fraction distributions in the surface at this stage is shown in Fig. 5b, c, where almost no phase transformation happens in the center. This manifests that even near the maximum strain area, only some elements undergo martensitic transformation. This phenomenon starts to change after the interconnect is stretched to a straight line. At this stage, martensitic transformation happens over the entire structure and martensite volume fraction starts to increase rapidly. The last stage happens when ε_{max} exceeds ε_{ela} of Ni-Ti alloy, where the applied strain reaches 196%, and plastic deformation begins to occur. From the above discussion, we can conclude that as long as the applied strain is less than 196%, the deformation is within the elastic range, and could completely recover by reverse phase transformation after releasing applied strain.

Electrical properties of the Ni-Ti serpentine interconnects and assembling of LED arrays

Besides mechanical properties, electrical properties, including conductivity and resistance stability, are also very important for the electrical interconnect. The electrical resistivity of Ni-Ti alloys depends on its composition and phase state[20,21], and that of the austenite is usually in the range of 70 – 140 μΩ•cm, corresponding to the electrical conductivity of 7.1×10^5 – 1.4×10^6 S m^{-1}. By our measurements and calculations, the conductivity of Ni-Ti interconnects with a diameter of 30 μm reported in this work is ~8.6×10^5 S m^{-1}, which is consistent with the conductivity range reported by literatures.

The relative resistance change for Ni-Ti serpentine interconnect with respect to the applied strain is shown in Fig. 6a. The relative resistance change is defined as $(R - R_0)/R_0$, where R and R_0 indicate the electrical resistances with and without the tensile strain, respectively. We observe that upon applying 175% tensile strain, the relative resistance change for the interconnect is only 2.8% and there is a negligible electrical hysteresis during applying and releasing strain. From the classical law of resistance, the resistance of the Ni-Ti interconnect can be expressed as

$$R = \rho \frac{L}{A}, \quad (1)$$

Where ρ is the resistivity of the Ni-Ti alloy, L and A are the length and cross-sectional area of the ρ interconnect, respectively. Therefore, the relative change of resistance can be rewritten by

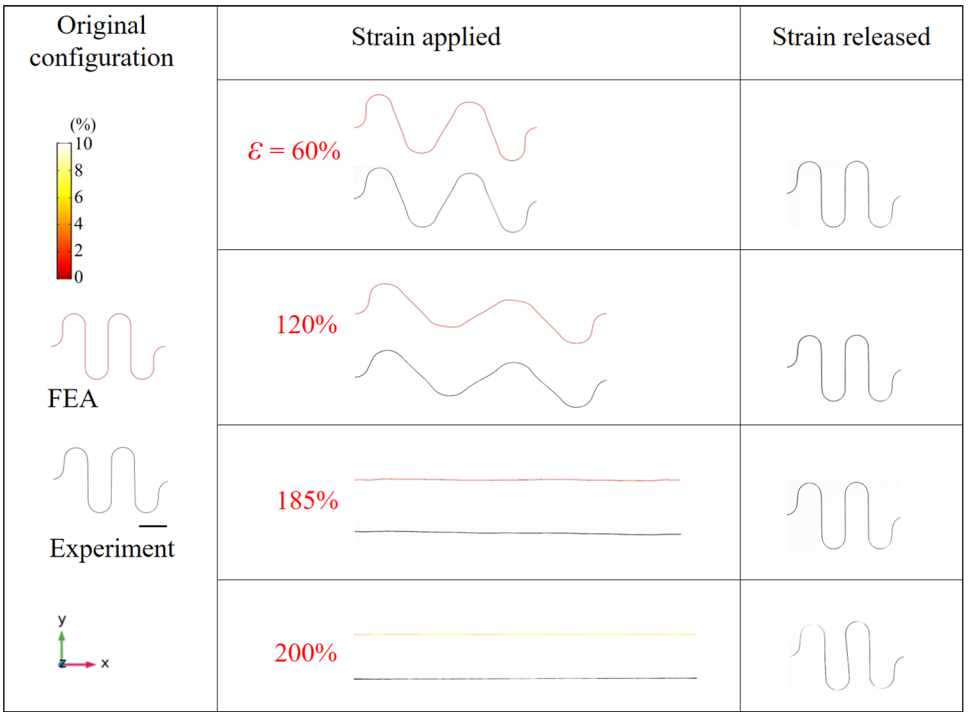

Fig. 4 Stretchable experiments and simulations. The middle column shows optical images (gray image) and their corresponding FEA simulation results (color image) for the interconnect under different applied tensile strain. The right column shows the interconnect structures after releasing the applied strain. The scale bar is 2 mm.

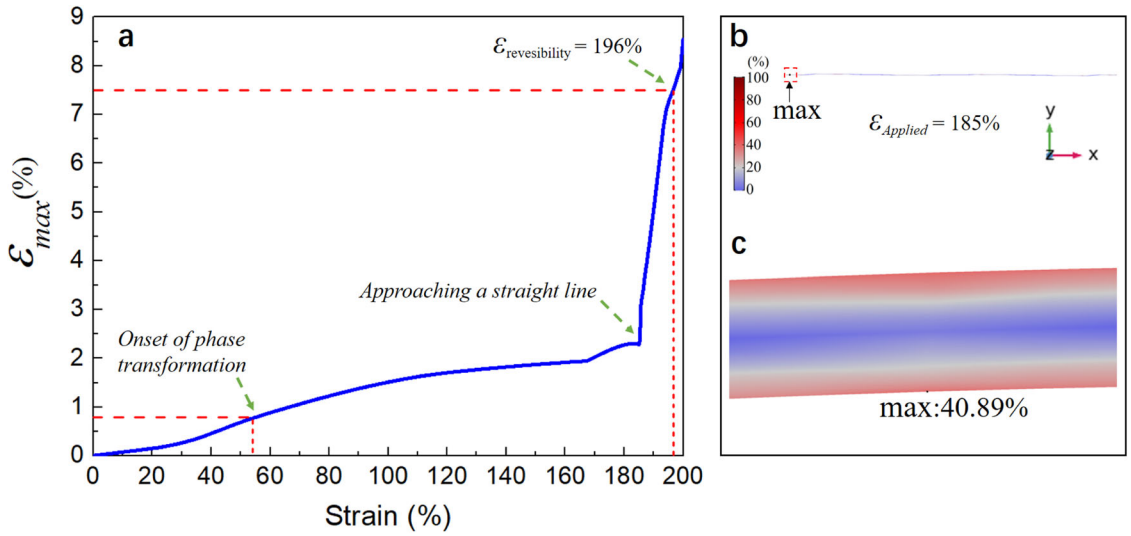

Fig. 5 Discussion of FEA simulation results. a Dependence of the maximum principal strain, ε_{max}, (on the material level) on the applied strain, ε_{app}, (on the structure level). **b** FEA simulation of the martensite volume fraction distribution under the applied tensile strain of 185%. **c** Magnified view of modeling results for the part of the interconnect structures that experience the highest strain.

taking the total derivative of Eq. (1) and simplified as

$$\frac{dR}{R} = \frac{d\rho}{\rho} + (1 + 2\mu)\frac{\Delta L}{L}. \quad (2)$$

where μ and ΔL are Poisson's ratio of the material and the length change of the interconnect, respectively. Since unfolding is the main deformation mode before the serpentine interconnect is stretched into a straight line, the length change, ΔL, can be ignored before applying 185% tensile strain, and the resistance change mainly comes from the resistivity change resulting from the phase transformation. As discussed before, there is almost no martensitic transition before applying 54% strain, which can explain why negligible resistance change is observed at this stage. When the applied strain increases, the martensitic transformation happens and the interconnect resistance starts to increase since the resistivity of martensite, ρ_M, is higher than that of austenite, ρ_A [22]. Due to the low strain level and the localized characteristics of strain distribution in the interconnect, the electrical resistance changes by only 0.4% with 100% strain.

In order to verify the electrical resistance stability of the interconnect against repetitive deformation, cyclical stretching from $\varepsilon = 0$ to 100% with a frequency of 0.025 Hz is applied to the

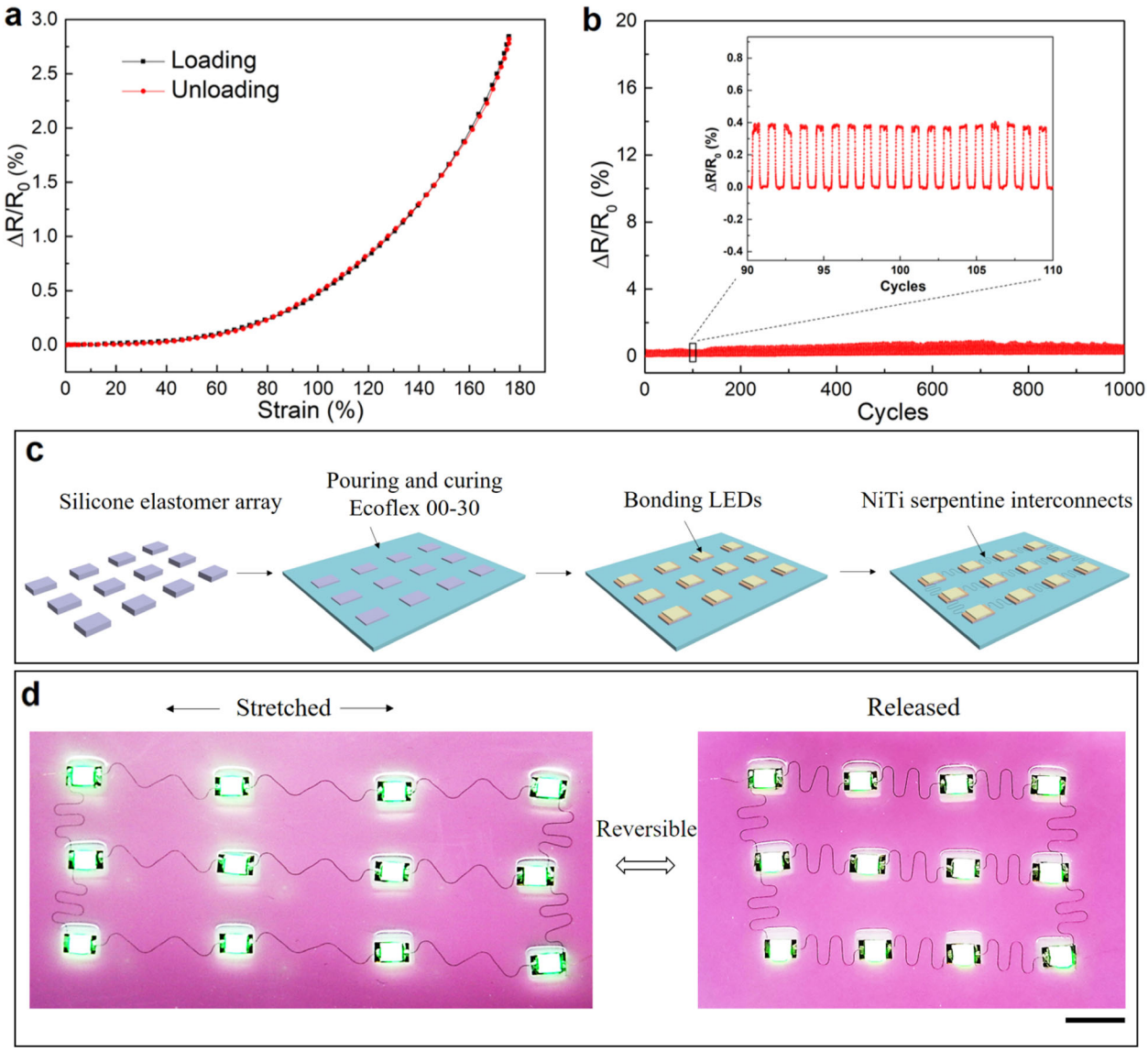

Fig. 6 Electrical properties and stretchable LED array device. a Relative resistance change of the Ni-Ti interconnect as a function of applied strain, showing a negligible hysteresis behavior when loading and unloading. **b** Relative resistance change under cyclic stretching from $\varepsilon = 0\%$ to $\varepsilon = 100\%$ with a frequency of 0.025 Hz over 1000 cycles, the inset shows a zoomed-in image of relative resistance change between cycle 90 and 110. **c** Stretchable LED array device fabrication flow chart. **d** Optical image of the LED array device under stretching, the scale bar is 10 mm. Pink paper was used as the background to make the interconnects clear.

interconnect for 1000 cycles and its relative electrical resistance variation is measured. As shown in Fig. 6b, the relative change of resistance follows the same trend during each cycle and it only varies by 1% after the interconnect is subjected to 100% strain deformation over 1000 cycles. In addition, the interconnect would recover to its initial configuration without any noticeable degradation after the stretching cycles are complete, which demonstrates the high durability and reliability of the serpentine interconnect based on Ni-Ti alloy.

From the above results and analysis, we conclude that serpentine interconnects based on superelastic Ni-Ti alloy exhibit high elastic stretchability and stable electrical resistance, which facilitate its usage as electrical interconnects for stretchable electronics. To better illustrate this, we integrate LEDs on a stretchable substrate and connect them with Ni-Ti serpentine interconnects. The substrate consists of rigid silicone elastomer islands embedded in a soft Ecoflex 00-30 elastomer, and the manufacturing process is shown in Fig. 6c. Since the modulus of silicone elastomer is much higher than that of Ecoflex 00-30, the hard-on-soft structure could provide strain protection for the mechanically rigid islands by isolating them from the applied macroscopic strain. The as-fabricated LED array are shown in Fig. 6d, which could be reversibly stretched as shown in Fig. 6d and Supplementary Movie 6.

Discussion of the potentials and challenges of other superelastic alloys as electrical interconnects

The above results verify that it is feasible to enhance the elastic stretchability of electrical interconnect by superelastic SMAs. Here, it should be noted that Cu serpentine interconnects in literature are usually in the form of flat strips[7,8]. Based on the above results and principle, it can be predicted that flat serpentine interconnects made by superelastic Ni-Ti alloys will also possess higher elastic stretchability than that made by conventional metals. In order to be more conveniently integrated into a well-established electronic manufacturing process, other methods are needed to

make superelastic alloy-based electrical interconnects. So far, there are two potential methods, one is sputtering[3,7], the other is laser cutting or etching of thin foils[6,8]. The former method requires precisely controlling the composition and microstructure of the film to ensure its superelastic state. The latter method normally requires the fabrication of superelastic alloy foil with thickness less than 100 μm, which remains a challenge due to its low plastic workability[23]. Therefore, more efforts are needed to fabricate superelastic alloy-based electrical interconnects for stretchable electronics. On the other hand, except for the typical Ni-Ti alloy, other superelastic alloys including Cu-based, e.g., Cu-Al-Mn[24–26], Cu-Al-Ni[27,28], and Fe-based SMAs, e.g., Fe-Mn-Si[29], Fe-Mn-Al-Ni[30,31], can be exploited to make electrical interconnects. In particular, Cu-based SMAs with high conductivity would be an ideal material for highly elastic electrical interconnects. For Fe-based SMAs, great progress in superelastic properties has been made in the past 10 years[29–31], which makes it a potential material for stretchable interconnect design.

In summary, from the perspective of the relationship between the elastic stretchability of structured interconnect and the intrinsic elastic strain limit of the material, we propose to exploit material of superelastic alloys to enhance the elastic stretchability of interconnects. Serpentine interconnect made by superelastic Ni-Ti alloy with elastic strain limit of 7.5% represents a much higher elastic stretchability than Cu interconnect. Detailed deformation information, including strain distribution and phase transition of Ni-Ti serpentine structures, are systematically studied through experiments and FEA simulations. The elastic stretchability of the serpentine interconnect is predicted to be 196%, and the stretching process could be divided into four stages according to the spatial distribution and extent of phase transformation. Due to the low strain level and the localized characteristics of the strain distribution in the interconnect, the electrical resistance only changes by 0.4% with 100% strain. The mechanical and electrical properties of the Ni-Ti interconnect facilitate its utilization as interconnects for stretchable electronics. The proposed superelastic alloys fundamentally boost the stretchable properties of electrical interconnects, which would open up opportunities for flexible and stretchable electronics.

METHODS

Fabrication of serpentine interconnects based on Ni-Ti alloys

The fabrication process is shown in Fig. 2a. Firstly, a superelastic straight Ni-Ti wire with a nominal composition of $Ni_{50.9}Ti_{49.1}$ (Jiangyin Hao Lu Ni-Ti New Material Co. LTD) is put in the serpentine groove of the mold, and covered by a stainless plate. The mold is then put into a tube furnace and annealed at 500 °C for 20 min under argon atmosphere before water quenching to room temperature. The images of the original straight Ni-Ti wire and the serpentine interconnect after heat setting are shown in Supplementary Fig. 2. A length of straight Ni-Ti wire is put into the furnace for heat treatment at the same time, which is used for mechanical and thermal characterization.

Comparison of stretchability between Cu and Ni-Ti serpentine interconnect

Cu serpentine interconnects of the same size as Ni-Ti interconnects are made by setting wires with a mask. The Cu and Ni-Ti serpentine interconnects are stretched in a stepper machine (Beijing Optical Century Instrument Co., Ltd., China) with one end fixed and the other end elongated and recovered, while a digital camera (Canon EOS 70D) is used to take the optical photographs and videos.

Mechanical and thermal properties of Ni-Ti alloy

Mechanical and thermal properties of Ni-Ti wires are characterized by the dynamic mechanical analyzer (DMA) and differential scanning calorimetry (DSC). Uniaxial tensile tests for the heat-treated Ni-Ti straight wires with a diameter of 30 μm, with a strain rate of 0.5 mm/min and a gauge length of ~15 mm, are carried out in DMA (TA Instruments Q850). Loading-unloading tests are performed with various levels of tensile strain at room temperature. In addition, temperature-dependent loading-unloading tests are performed (Supplementary Fig. 3). As shown in Supplementary Fig. 4, the characteristic parameters of C_M and C_A could be obtained by linear fitting the critical stresses versus temperatures curve. DSC is conducted at a heating/cooling rate of 5 °C/min to obtain phase transformation temperatures as shown in Fig. 3d. All mechanical and thermal properties for Ni-Ti are summarized in Supplementary Table 2.

FEA simulations of the deformation for Ni-Ti serpentine interconnect

The dimensions of the model are shown in Supplementary Fig. 1b, with a length of 8.25 mm in the X direction and a diameter of 30 μm. The model is built by connecting several isolated parts to form a consortium, and in order to avoid the inability to calculate some unusable units after meshing, virtual geometry was used to make all parts form a complex area, where some surfaces and closed edge lines which are too small to be calculated were ignored. Then the model is set as a shape memory alloy in the physical field of solid mechanics with the parameters presented in Supplementary Table 2. After that, by using the free triangular mesh as shown in Supplementary Fig. 5, the cross-section and the length of the model is divided into 8 pieces and 200 pieces, respectively. Then the left end of the model is set to be fixed as the constraint condition and the deformation length step of the right end at the X-axis is set as 0.05%. In FEA, the original strain tensor, E, when ignoring the quadratic terms, can just be used to describe the situation of small strain and rigid body rotation. For conditions of high stretchability and rotation deformation in this work, we changed the related parameters in the equation by adding the quadratic terms. So, the strain tensor, E, can be described as

$$E_{ij} = \frac{1}{2}\left(\frac{\partial u_i}{\partial X_j} + \frac{\partial u_j}{\partial X_i} + \frac{\partial u_k}{\partial X_i}\frac{\partial u_k}{\partial X_j}\right), \tag{3}$$

$$E_{ii} = \frac{\partial u_i}{\partial X_i} + \frac{1}{2}\left\{\left(\frac{\partial u_i}{\partial X_i}\right)^2 + \left(\frac{\partial u_j}{\partial X_i}\right)^2 + \left(\frac{\partial u_k}{\partial X_i}\right)^2\right\}, \tag{4}$$

where X and u represents the location and displacement in the coordinate system. By solving the equations, the evolution of deformed configurations and martensite volume fraction contour with applied strains are obtained, as shown in Fig. 4 and Supplementary Fig. 6, respectively.

Resistance measurements of Ni-Ti serpentine interconnect during deformation

Ni-Ti serpentine interconnects are stretched in the same stepper machine, while the displacement and the resistance are recorded at the same time by a laser displacement sensor (Keyence, LK-H052) and a digital source meter (Keithley 2602 A) under a constant voltage (V_0) of 0.5 V, respectively.

Assembly of LEDs connected by Ni-Ti serpentine interconnects

Figure 6c illustrates the manufacturing process of stretchable LED array devices. Firstly, the silicone elastomer is cut into several pieces of cuboids with a size of 5 mm × 3 mm × 1.5 mm, and placed in a dish in an array. Then Ecoflex™ 00-30 silicone (Smooth-On, Inc.), with a base to curing agent weight ratio of 1:1, is poured into the dish. After curing at room temperature for 6 h, a soft elastomer embedded with rigid silicone elastomer islands is formed. Finally, LEDs are fixed on the islands by epoxy resin and the Ni-Ti serpentine interconnects are used to connect both ends of the LEDs.

DATA AVAILABILITY

All data that support the findings of this study are available from the corresponding author upon reasonable request.

Received: 11 October 2021; Accepted: 21 December 2021;
Published online: 03 February 2022

REFERENCES

1. Wang, C., Wang, C., Huang, Z. & Xu, S. Materials and structures toward soft electronics. *Adv. Mater.* **30**, 1801368 (2018).

2. Xue, Z., Song, H., Rogers, J. A., Zhang, Y. & Huang, Y. Mechanically-guided structural designs in stretchable inorganic electronics. *Adv. Mater.* **32**, 1902254 (2020).
3. Xu, S. et al. Soft microfluidic assemblies of sensors, circuits and radios for the skin. *Science* **70**, 70–74 (2014).
4. Fu, H. et al. Lateral buckling and mechanical stretchability of fractal interconnects partially bonded onto an elastomeric substrate. *Appl. Phys. Lett.* **106**, 091902 (2015).
5. Zhang, Y. et al. Mechanics of ultra-stretchable selt-similar serpentine interconnects. *Acta Mater.* **61**, 7816–7827 (2013).
6. Huang, Z. et al. Three-dimensional integrated stretchable electronics. *Nat. Electron.* **1**, 473–480 (2018).
7. Xu, S. et al. Stretchable batteries with self-similar serpentine interconnects and integrated wireless recharging systems. *Nat. Commun.* **4**, 1543 (2013).
8. Wang, C. et al. Monitoring of the central blood pressure waveform via a conformal ultrasonic device. *Nat. Biomed. Eng.* **2**, 687–695 (2018).
9. Yoo, J., Jeong, S., Kim, S. & Je, J. H. A stretchable nanowire UV-Vis-NIR photodetector with high performance. *Adv. Mater.* **27**, 1712–1717 (2015).
10. Zhang, Y. et al. Buckling in serpentine microstructures and applications in elastomer-supported ultra-stretchable electronics with high areal coverage. *Soft Matter* **9**, 8062–8070 (2013).
11. Koshi, T., Nomura, K. & Yoshida, M. Measurement and analysis on failure lifetime of serpentine interconnects for e-textiles under cyclic large deformation. *Flex. Print. Eletron* **6**, 025003 (2021).
12. Nie, S., Cai, M., Wang, C. & Song, J. Fatigue life prediction of serpentine interconnects on soft elastomers for stretchable electronics. *J. Appl. Mech.* **87**, 011011 (2020).
13. Kim, D. et al. Materials and noncoplanar mesh designs for integrated circuits with linear elastic responses to extreme mechanical deformations. *Proc. Natl Acad. Sci. USA* **105**, 18675–18680 (2008).
14. Rojas, J. P., Arevalo, A., Foulds, I. G. & Hussain, M. M. Design and characterization of ultra-stretchable monolithic silicon fabric. *Appl. Phys. Lett.* **105**, 154101 (2014).
15. Nan, K. et al. Compliant and stretchable thermoelectric coils for energy harvesting in miniature flexible devices. *Sci. Adv.* **4**, eaau5849 (2018).
16. Jang, K. et al. Self-assembled three dimensional network designs for soft electronics. *Nat. Commun.* **8**, 15894 (2017).
17. Hochrainer, T. et al. Continuum dislocation dynamics: towards a physical theory of crystal plasticicty. *J. Mech. Phys. Solids* **63**, 167–178 (2014).
18. Tadaki, T., Otsuka, K. & Shimizu, K. Shape memory alloys. *Annu. Rev. Mater. Sci.* **18**, 25–45 (1988).
19. Jani, J. M., Leary, M., Subic, A. & Gibson, M. A. A review of shape memory alloy research, applications and opportunities. *Mater. Des.* **56**, 1078–1113 (2014).
20. Lee, J. Y. et al. Thermopower behavior for the shape memory alloy NiTi. *J. Appl. Phys.* **89**, 6223 (2001).
21. Ingale, B. D., Wei, W. C., Chang, P. C., Kuo, Y. K. & Wu, S. K. Anomalous transport and thermal properties of NiTi and with Cu an Fe-doped shape memory alloys near the martensitic transition. *J. Appl. Phys.* **110**, 113721 (2011).
22. Airoldi, G. & Pozzi, M. The electrical transport properties of shape memory alloys under a stress state. *J. Eng. Mater. Technol.* **121**, 108–111 (1999).
23. Tomus, D., Tsuchiya, K. & Inuzuka, M. Fabrication of shape memory TiNi foils via Ti/Ni ultrafine laminates. *Scr. Mater.* **48**, 489–494 (2003).
24. Kusama, T. et al. Ultra-large single crystals by abnormal grain growth. *Nat. Commun.* **8**, 354 (2017).
25. Omori, T. et al. Abnormal grain growth induced by cyclic heat treatment. *Science* **341**, 1500–1502 (2013).
26. Sutou, Y., Omori, T., Kainuma, R. & Ishida, K. Grain size dependence of pseudoelasticity in polycrystalline Cu-Al-Mn-based shape memory sheets. *Acta Mater.* **61**, 3842–3850 (2013).
27. Morána, M. J., Condó, A. M. & Haberkorn, N. Recrystallization and martensitic transformation in nanometric grain size Cu-Al-Ni thin films grown by DC sputtering at room temperature. *Mater. Charact.* **139**, 446–451 (2018).
28. Ueland, S. M., Chen, Y. & Schuh, C. A. Oligocrystalline shape memory alloys. *Adv. Funct. Mater.* **22**, 2094–2099 (2012).
29. Wen, Y. H. et al. Large recovery strain in Fe-Mn-Si-based shape memory steels obtained by engineering annealing twin boundaries. *Nat. Commun.* **5**, 4964 (2014).
30. Tanaka, Y. et al. Ferrous polycrystalline shape-memory alloy showing huge superelasticity. *Science* **327**, 1488–1490 (2010).
31. Omori, T. et al. Superelastic effect in polycrystalline ferrous alloys. *Science* **333**, 68–71 (2011).

ACKNOWLEDGEMENTS

The authors acknowledge the funding support from the National Key R&D Program of China (2020YFB2008501), the Natural Science Foundation of Jiangsu Province (BK20200259), the National Natural Science Foundation of China (62071463), and the National Science Fund for Distinguished Young Scholars (62125112). The authors are grateful for the technical support for Nano-X from Suzhou Institute of Nano-Tech and Nano-Bionics, Chinese Academy of Sciences (SINANO).

AUTHOR CONTRIBUTIONS

Y.Z. and W.Z. contributed equally to this work. Y.Z. designed, fabricated, and characterized the electric interconnects and devices. W.Z. carried out FEA simulations. Y.S., X.Y., Y.B., and L.L. participated in the device fabrications and electrical measurements. S.W., T.L., and S.F. helped with manuscript figures and writing. T.Z. conceived of the work and coordinated the research. All authors contributed to the scientific planning and discussion.

COMPETING INTERESTS

The authors declare no competing interests.

ADDITIONAL INFORMATION

Supplementary information The online version contains supplementary material available at https://doi.org/10.1038/s41528-022-00142-2.

Correspondence and requests for materials should be addressed to Ting Zhang.

Reprints and permission information is available at http://www.nature.com/reprints

Publisher's note Springer Nature remains neutral with regard to jurisdictional claims in published maps and institutional affiliations.